Measurements of WW and WZ Production in W+jets Final States in pp[over ¯] Collisions

V. M. Abazov *et al.* (D0 Collaboration)

Phys. Rev. Lett. **108**, 181803 — Published 2 May 2012
DOI: 10.1103/PhysRevLett.108.181803

Fermilab-Pub-11/635-E

Measurements of WW and WZ production in W + jets final states in $p\bar{p}$ collisions

V.M. Abazov,[34] B. Abbott,[72] B.S. Acharya,[28] M. Adams,[48] T. Adams,[46] G.D. Alexeev,[34] G. Alkhazov,[38] A. Alton[a],[60] G. Alverson,[59] G.A. Alves,[2] M. Aoki,[47] A. Askew,[46] B. Åsman,[40] S. Atkins,[57] O. Atramentov,[64] K. Augsten,[9] C. Avila,[7] J. BackusMayes,[79] F. Badaud,[12] L. Bagby,[47] B. Baldin,[47] D.V. Bandurin,[46] S. Banerjee,[28] E. Barberis,[59] P. Baringer,[55] J. Barreto,[3] J.F. Bartlett,[47] U. Bassler,[17] V. Bazterra,[48] A. Bean,[55] M. Begalli,[3] C. Belanger-Champagne,[40] L. Bellantoni,[47] S.B. Beri,[26] G. Bernardi,[16] R. Bernhard,[21] I. Bertram,[41] M. Besançon,[17] R. Beuselinck,[42] V.A. Bezzubov,[37] P.C. Bhat,[47] V. Bhatnagar,[26] G. Blazey,[49] S. Blessing,[46] K. Bloom,[63] A. Boehnlein,[47] D. Boline,[69] E.E. Boos,[36] G. Borissov,[41] T. Bose,[58] A. Brandt,[75] O. Brandt,[22] R. Brock,[61] G. Brooijmans,[67] A. Bross,[47] D. Brown,[16] J. Brown,[16] X.B. Bu,[47] M. Buehler,[47] V. Buescher,[23] V. Bunichev,[36] S. Burdin[b],[41] T.H. Burnett,[79] C.P. Buszello,[40] B. Calpas,[14] E. Camacho-Pérez,[31] M.A. Carrasco-Lizarraga,[55] B.C.K. Casey,[47] H. Castilla-Valdez,[31] S. Chakrabarti,[69] D. Chakraborty,[49] K.M. Chan,[53] A. Chandra,[77] E. Chapon,[17] G. Chen,[55] S. Chevalier-Théry,[17] D.K. Cho,[74] S.W. Cho,[30] S. Choi,[30] B. Choudhary,[27] S. Cihangir,[47] D. Claes,[63] J. Clutter,[55] M. Cooke,[47] W.E. Cooper,[47] M. Corcoran,[77] F. Couderc,[17] M.-C. Cousinou,[14] A. Croc,[17] D. Cutts,[74] A. Das,[44] G. Davies,[42] K. De,[75] S.J. de Jong,[33] E. De La Cruz-Burelo,[31] F. Déliot,[17] R. Demina,[68] D. Denisov,[47] S.P. Denisov,[37] S. Desai,[47] C. Deterre,[17] K. DeVaughan,[63] H.T. Diehl,[47] M. Diesburg,[47] P.F. Ding,[43] A. Dominguez,[63] T. Dorland,[79] A. Dubey,[27] L.V. Dudko,[36] D. Duggan,[64] A. Duperrin,[14] S. Dutt,[26] A. Dyshkant,[49] M. Eads,[63] D. Edmunds,[61] J. Ellison,[45] V.D. Elvira,[47] Y. Enari,[16] H. Evans,[51] A. Evdokimov,[70] V.N. Evdokimov,[37] G. Facini,[59] T. Ferbel,[68] F. Fiedler,[23] F. Filthaut,[33] W. Fisher,[61] H.E. Fisk,[47] M. Fortner,[49] H. Fox,[41] S. Fuess,[47] A. Garcia-Bellido,[68] G.A García-Guerra[c],[31] V. Gavrilov,[35] P. Gay,[12] W. Geng,[14,61] D. Gerbaudo,[65] C.E. Gerber,[48] Y. Gershtein,[64] G. Ginther,[47,68] G. Golovanov,[34] A. Goussiou,[79] P.D. Grannis,[69] S. Greder,[18] H. Greenlee,[47] Z.D. Greenwood,[57] E.M. Gregores,[4] G. Grenier,[19] Ph. Gris,[12] J.-F. Grivaz,[15] A. Grohsjean,[17] S. Grünendahl,[47] M.W. Grünewald,[29] T. Guillemin,[15] G. Gutierrez,[47] P. Gutierrez,[72] A. Haas[d],[67] S. Hagopian,[46] J. Haley,[59] L. Han,[6] K. Harder,[43] A. Harel,[68] J.M. Hauptman,[54] J. Hays,[42] T. Head,[43] T. Hebbeker,[20] D. Hedin,[49] H. Hegab,[73] A.P. Heinson,[45] U. Heintz,[74] C. Hensel,[22] I. Heredia-De La Cruz,[31] K. Herner,[60] G. Hesketh[e],[43] M.D. Hildreth,[53] R. Hirosky,[78] T. Hoang,[46] J.D. Hobbs,[69] B. Hoeneisen,[11] M. Hohlfeld,[23] Z. Hubacek,[9,17] V. Hynek,[9] I. Iashvili,[66] Y. Ilchenko,[76] R. Illingworth,[47] A.S. Ito,[47] S. Jabeen,[74] M. Jaffré,[15] D. Jamin,[14] A. Jayasinghe,[72] R. Jesik,[42] K. Johns,[44] M. Johnson,[47] A. Jonckheere,[47] P. Jonsson,[42] J. Joshi,[26] A.W. Jung,[47] A. Juste,[39] K. Kaadze,[56] E. Kajfasz,[14] D. Karmanov,[36] P.A. Kasper,[47] I. Katsanos,[63] R. Kehoe,[76] S. Kermiche,[14] N. Khalatyan,[47] A. Khanov,[73] A. Kharchilava,[66] Y.N. Kharzheev,[34] J.M. Kohli,[26] A.V. Kozelov,[37] J. Kraus,[61] S. Kulikov,[37] A. Kumar,[66] A. Kupco,[10] T. Kurča,[19] V.A. Kuzmin,[36] J. Kvita,[8] S. Lammers,[51] G. Landsberg,[74] P. Lebrun,[19] H.S. Lee,[30] S.W. Lee,[54] W.M. Lee,[47] J. Lellouch,[16] L. Li,[45] Q.Z. Li,[47] S.M. Lietti,[5] J.K. Lim,[30] D. Lincoln,[47] J. Linnemann,[61] V.V. Lipaev,[37] R. Lipton,[47] Y. Liu,[6] A. Lobodenko,[38] M. Lokajicek,[10] R. Lopes de Sa,[69] H.J. Lubatti,[79] R. Luna-Garcia[f],[31] A.L. Lyon,[47] A.K.A. Maciel,[2] D. Mackin,[77] R. Madar,[17] R. Magaña-Villalba,[31] S. Malik,[63] V.L. Malyshev,[34] Y. Maravin,[56] J. Martínez-Ortega,[31] R. McCarthy,[69] C.L. McGivern,[55] M.M. Meijer,[33] A. Melnitchouk,[62] D. Menezes,[49] P.G. Mercadante,[4] M. Merkin,[36] A. Meyer,[20] J. Meyer,[22] F. Miconi,[18] N.K. Mondal,[28] G.S. Muanza,[14] M. Mulhearn,[78] E. Nagy,[14] M. Naimuddin,[27] M. Narain,[74] R. Nayyar,[27] H.A. Neal,[60] J.P. Negret,[7] P. Neustroev,[38] S.F. Novaes,[5] T. Nunnemann,[24] G. Obrant[‡],[38] J. Orduna,[77] N. Osman,[14] J. Osta,[53] G.J. Otero y Garzón,[1] M. Padilla,[45] A. Pal,[75] N. Parashar,[52] V. Parihar,[74] S.K. Park,[30] R. Partridge[d],[74] N. Parua,[51] A. Patwa,[70] B. Penning,[47] M. Perfilov,[36] Y. Peters,[43] K. Petridis,[43] G. Petrillo,[68] P. Pétroff,[15] R. Piegaia,[1] M.-A. Pleier,[70] P.L.M. Podesta-Lerma[g],[31] V.M. Podstavkov,[47] P. Polozov,[35] A.V. Popov,[37] M. Prewitt,[77] D. Price,[51] N. Prokopenko,[37] J. Qian,[60] A. Quadt,[22] B. Quinn,[62] M.S. Rangel,[2] K. Ranjan,[27] P.N. Ratoff,[41] I. Razumov,[37] P. Renkel,[76] M. Rijssenbeek,[69] I. Ripp-Baudot,[18] F. Rizatdinova,[73] M. Rominsky,[47] A. Ross,[41] C. Royon,[17] P. Rubinov,[47] R. Ruchti,[53] G. Safronov,[35] G. Sajot,[13] P. Salcido,[49] A. Sánchez-Hernández,[31] M.P. Sanders,[24] B. Sanghi,[47] A.S. Santos,[5] G. Savage,[47] L. Sawyer,[57] T. Scanlon,[42] R.D. Schamberger,[69] Y. Scheglov,[38] H. Schellman,[50] T. Schliephake,[25] S. Schlobohm,[79] C. Schwanenberger,[43] R. Schwienhorst,[61] J. Sekaric,[55] H. Severini,[72] E. Shabalina,[22] V. Shary,[17] A.A. Shchukin,[37] R.K. Shivpuri,[27] V. Simak,[9] V. Sirotenko,[47] P. Skubic,[72] P. Slattery,[68] D. Smirnov,[53] K.J. Smith,[66] G.R. Snow,[63] J. Snow,[71] S. Snyder,[70]

S. Söldner-Rembold,[43] L. Sonnenschein,[20] K. Soustruznik,[8] J. Stark,[13] V. Stolin,[35] D.A. Stoyanova,[37] M. Strauss,[72] D. Strom,[48] L. Stutte,[47] L. Suter,[43] P. Svoisky,[72] M. Takahashi,[43] A. Tanasijczuk,[1] M. Titov,[17] V.V. Tokmenin,[34] Y.-T. Tsai,[68] K. Tschann-Grimm,[69] D. Tsybychev,[69] B. Tuchming,[17] C. Tully,[65] L. Uvarov,[38] S. Uvarov,[38] S. Uzunyan,[49] R. Van Kooten,[51] W.M. van Leeuwen,[32] N. Varelas,[48] E.W. Varnes,[44] I.A. Vasilyev,[37] P. Verdier,[19] L.S. Vertogradov,[34] M. Verzocchi,[47] M. Vesterinen,[43] D. Vilanova,[17] P. Vokac,[9] H.D. Wahl,[46] M.H.L.S. Wang,[47] J. Warchol,[53] G. Watts,[79] M. Wayne,[53] M. Weber[h],[47] L. Welty-Rieger,[50] A. White,[75] D. Wicke,[25] M.R.J. Williams,[41] G.W. Wilson,[55] M. Wobisch,[57] D.R. Wood,[59] T.R. Wyatt,[43] Y. Xie,[47] R. Yamada,[47] W.-C. Yang,[43] T. Yasuda,[47] Y.A. Yatsunenko,[34] Z. Ye,[47] H. Yin,[47] K. Yip,[70] S.W. Youn,[47] J. Yu,[75] T. Zhao,[79] B. Zhou,[60] J. Zhu,[60] M. Zielinski,[68] D. Zieminska,[51] and L. Zivkovic[74]

(The D0 Collaboration*)

[1]*Universidad de Buenos Aires, Buenos Aires, Argentina*
[2]*LAFEX, Centro Brasileiro de Pesquisas Físicas, Rio de Janeiro, Brazil*
[3]*Universidade do Estado do Rio de Janeiro, Rio de Janeiro, Brazil*
[4]*Universidade Federal do ABC, Santo André, Brazil*
[5]*Instituto de Física Teórica, Universidade Estadual Paulista, São Paulo, Brazil*
[6]*University of Science and Technology of China, Hefei, People's Republic of China*
[7]*Universidad de los Andes, Bogotá, Colombia*
[8]*Charles University, Faculty of Mathematics and Physics, Center for Particle Physics, Prague, Czech Republic*
[9]*Czech Technical University in Prague, Prague, Czech Republic*
[10]*Center for Particle Physics, Institute of Physics, Academy of Sciences of the Czech Republic, Prague, Czech Republic*
[11]*Universidad San Francisco de Quito, Quito, Ecuador*
[12]*LPC, Université Blaise Pascal, CNRS/IN2P3, Clermont, France*
[13]*LPSC, Université Joseph Fourier Grenoble 1, CNRS/IN2P3, Institut National Polytechnique de Grenoble, Grenoble, France*
[14]*CPPM, Aix-Marseille Université, CNRS/IN2P3, Marseille, France*
[15]*LAL, Université Paris-Sud, CNRS/IN2P3, Orsay, France*
[16]*LPNHE, Universités Paris VI and VII, CNRS/IN2P3, Paris, France*
[17]*CEA, Irfu, SPP, Saclay, France*
[18]*IPHC, Université de Strasbourg, CNRS/IN2P3, Strasbourg, France*
[19]*IPNL, Université Lyon 1, CNRS/IN2P3, Villeurbanne, France and Université de Lyon, Lyon, France*
[20]*III. Physikalisches Institut A, RWTH Aachen University, Aachen, Germany*
[21]*Physikalisches Institut, Universität Freiburg, Freiburg, Germany*
[22]*II. Physikalisches Institut, Georg-August-Universität Göttingen, Göttingen, Germany*
[23]*Institut für Physik, Universität Mainz, Mainz, Germany*
[24]*Ludwig-Maximilians-Universität München, München, Germany*
[25]*Fachbereich Physik, Bergische Universität Wuppertal, Wuppertal, Germany*
[26]*Panjab University, Chandigarh, India*
[27]*Delhi University, Delhi, India*
[28]*Tata Institute of Fundamental Research, Mumbai, India*
[29]*University College Dublin, Dublin, Ireland*
[30]*Korea Detector Laboratory, Korea University, Seoul, Korea*
[31]*CINVESTAV, Mexico City, Mexico*
[32]*Nikhef, Science Park, Amsterdam, the Netherlands*
[33]*Radboud University Nijmegen, Nijmegen, the Netherlands and Nikhef, Science Park, Amsterdam, the Netherlands*
[34]*Joint Institute for Nuclear Research, Dubna, Russia*
[35]*Institute for Theoretical and Experimental Physics, Moscow, Russia*
[36]*Moscow State University, Moscow, Russia*
[37]*Institute for High Energy Physics, Protvino, Russia*
[38]*Petersburg Nuclear Physics Institute, St. Petersburg, Russia*
[39]*Institució Catalana de Recerca i Estudis Avançats (ICREA) and Institut de Física d'Altes Energies (IFAE), Barcelona, Spain*
[40]*Stockholm University, Stockholm and Uppsala University, Uppsala, Sweden*
[41]*Lancaster University, Lancaster LA1 4YB, United Kingdom*
[42]*Imperial College London, London SW7 2AZ, United Kingdom*
[43]*The University of Manchester, Manchester M13 9PL, United Kingdom*
[44]*University of Arizona, Tucson, Arizona 85721, USA*
[45]*University of California Riverside, Riverside, California 92521, USA*
[46]*Florida State University, Tallahassee, Florida 32306, USA*
[47]*Fermi National Accelerator Laboratory, Batavia, Illinois 60510, USA*
[48]*University of Illinois at Chicago, Chicago, Illinois 60607, USA*

[49]Northern Illinois University, DeKalb, Illinois 60115, USA
[50]Northwestern University, Evanston, Illinois 60208, USA
[51]Indiana University, Bloomington, Indiana 47405, USA
[52]Purdue University Calumet, Hammond, Indiana 46323, USA
[53]University of Notre Dame, Notre Dame, Indiana 46556, USA
[54]Iowa State University, Ames, Iowa 50011, USA
[55]University of Kansas, Lawrence, Kansas 66045, USA
[56]Kansas State University, Manhattan, Kansas 66506, USA
[57]Louisiana Tech University, Ruston, Louisiana 71272, USA
[58]Boston University, Boston, Massachusetts 02215, USA
[59]Northeastern University, Boston, Massachusetts 02115, USA
[60]University of Michigan, Ann Arbor, Michigan 48109, USA
[61]Michigan State University, East Lansing, Michigan 48824, USA
[62]University of Mississippi, University, Mississippi 38677, USA
[63]University of Nebraska, Lincoln, Nebraska 68588, USA
[64]Rutgers University, Piscataway, New Jersey 08855, USA
[65]Princeton University, Princeton, New Jersey 08544, USA
[66]State University of New York, Buffalo, New York 14260, USA
[67]Columbia University, New York, New York 10027, USA
[68]University of Rochester, Rochester, New York 14627, USA
[69]State University of New York, Stony Brook, New York 11794, USA
[70]Brookhaven National Laboratory, Upton, New York 11973, USA
[71]Langston University, Langston, Oklahoma 73050, USA
[72]University of Oklahoma, Norman, Oklahoma 73019, USA
[73]Oklahoma State University, Stillwater, Oklahoma 74078, USA
[74]Brown University, Providence, Rhode Island 02912, USA
[75]University of Texas, Arlington, Texas 76019, USA
[76]Southern Methodist University, Dallas, Texas 75275, USA
[77]Rice University, Houston, Texas 77005, USA
[78]University of Virginia, Charlottesville, Virginia 22901, USA
[79]University of Washington, Seattle, Washington 98195, USA
(Dated: December 1, 2011)

We study WW and WZ production with $\ell\nu qq$ ($\ell = e, \mu$) final states using data collected by the D0 detector at the Fermilab Tevatron Collider corresponding to 4.3 fb^{-1} of integrated luminosity from $p\bar{p}$ collisions at $\sqrt{s} = 1.96$ TeV. Assuming the ratio between the production cross sections $\sigma(WW)$ and $\sigma(WZ)$ as predicted by the standard model, we measure the total WV ($V = W, Z$) cross section to be $\sigma(WV) = 19.6\ ^{+3.2}_{-3.0}$ pb, and reject the background-only hypothesis at a level of 7.9 standard deviations. We also use b-jet discrimination to separate the WZ component from the dominant WW component. Simultaneously fitting WW and WZ contributions, we measure $\sigma(WW) = 15.9\ ^{+3.7}_{-3.2}$ pb and $\sigma(WZ) = 3.3\ ^{+4.1}_{-3.3}$ pb, which is consistent with the standard model predictions.

PACS numbers: 14.70.Fm, 14.70.Hp, 13.85.Ni, 13.85.Qk

The study of the production of VV ($V = W, Z$) boson pairs provides an important test of the electroweak sector of the standard model (SM). In $p\bar{p}$ collisions at $\sqrt{s} = 1.96$ TeV, the next-to-leading order (NLO) SM cross sections for these processes are $\sigma(WW) = 11.7 \pm 0.8$ pb, $\sigma(WZ) = 3.5 \pm 0.3$ pb and $\sigma(ZZ) = 1.4 \pm 0.1$ pb [1]. Measuring a significant departure in cross section or deviations in the predicted kinematic distributions would indicate the presence of anomalous gauge boson couplings [2] or new particles in extensions of the SM [3]. This analysis also provides a proving ground for the advanced analysis techniques used in low mass Higgs searches [4]. The production of VV in $p\bar{p}$ collisions at the Fermilab Tevatron Collider has been observed in fully leptonic decay modes [5] and more recently, in leptons+jets decay modes [6], where the combined $WW + WZ$ cross section was measured. In pp collisions at $\sqrt{s} = 7$ TeV at the LHC, diboson production has been studied using the fully leptonic decay modes [7].

In this Letter, we report observation of the associated production of a W boson that decays leptonically and a second vector boson that decays hadronically ($WV \to \ell\nu qq$; $\ell = e^{\pm}$ or $\mu^{\pm}$, and ν and q denote matter or anti-

*with visitors from [a]Augustana College, Sioux Falls, SD, USA, [b]The University of Liverpool, Liverpool, UK, [c]UPIITA-IPN, Mexico City, Mexico, [d]SLAC, Menlo Park, CA, USA, [e]University College London, London, UK, [f]Centro de Investigacion en Computacion - IPN, Mexico City, Mexico, [g]ECFM, Universidad Autonoma de Sinaloa, Culiacán, Mexico, and [h]Universität Bern, Bern, Switzerland. ‡Deceased.

matter as appropriate). The data used for this analysis correspond to 4.3 fb^{-1} of integrated luminosity collected between 2006 and 2009 by the D0 detector [8] at the Fermilab Tevatron Collider. The D0 detector dijet mass resolution for W/Z decays of $\approx 18\%$ results in significant overlap of $W \to qq$ and $Z \to qq$ dijet mass peaks. Therefore, we first consider WW and WZ simultaneously and measure the total WV cross section assuming the ratio of WW to WZ cross sections as predicted by the SM. We then apply b-jet identification to separate the WZ contribution, where the Z boson decays into $b\bar{b}$ pairs, from the dominant WW production.

Candidate events in the electron channel are required to satisfy a single electron trigger or a trigger requiring electrons and jets, which results in a combined trigger efficiency of $(98^{+2}_{-3})\%$ for the $e\nu qq$ event selection described below. A comprehensive suite of triggers in the muon channel, based on leptons, jets and their combination, achieves a trigger efficiency of $(95 \pm 5)\%$ for the $\mu\nu qq$ event selection.

To select $WV\to \ell\nu qq$ candidates, we require a single reconstructed electron (muon) with transverse momentum $p_T > 15$ GeV (20 GeV) and pseudorapidity $|\eta| < 1.1$ (2.0) [9], missing transverse energy $\not\!\!E_T > 20$ GeV, and two or three jets reconstructed using a cone algorithm [10]. The jets must have $p_T > 20$ GeV, $|\eta| < 2.5$, and at least two tracks within the jet cone [10] originating from the $p\bar{p}$ interaction vertex. Lepton candidates must be spatially matched to a track that originates from the primary $p\bar{p}$ interaction vertex and they must be isolated from energy depositions in the calorimeter and other tracks in the central tracking detector. To reduce background from processes that do not contain $W\to \ell\nu$, we require that the W transverse mass [11] is $M_T^{\ell\nu}$ (GeV) $> 40 - 0.5\not\!\!E_T$. In addition, we restrict $M_T^{\mu\nu} < 200$ GeV to suppress muon candidates with poorly measured momenta.

Signal and most of the background processes are modeled with Monte Carlo (MC) simulation. The signal events are generated with PYTHIA [12] using CTEQ6L1 parton distribution functions (PDFs) [13] and include all SM decays. The fixed-order matrix element (FOME) generator ALPGEN [14] with CTEQ6L1 PDF is used to generate W+jets, Z+jets, and $t\bar{t}$ events. The FOME generator COMPHEP [15] is used to produce single top-quark MC samples with CTEQ6M PDF [13]. Both ALPGEN and COMPHEP are interfaced to PYTHIA for parton showering and hadronization. The MC events undergo a GEANT-based [16] detector simulation and are reconstructed using the same algorithms as used for D0 data. The effect of multiple $p\bar{p}$ interactions is included by overlaying data events from random beam crossings on simulated events. The next-to-NLO (NNLO) cross section is used to normalize the Z+jets (light and heavy-flavor jets) [17]. The approximate NNLO cross section [18] is used to normalize the $t\bar{t}$ samples, while the single top-quark MC samples are normalized to the approximate next-to-NNLO cross section [19]. The normalization of the W+jets MC sample (for all flavor contributions) is determined from data. Additional NLO heavy-flavor corrections are calculated with MCFM [20] and applied to Z/W+heavy-flavor jets MC samples.

The multijet background in which a jet is misidentified as a prompt lepton is determined from data. For the muon channel, the multijet background is modeled with data that fail the muon isolation requirements, but pass all other selections. For the electron channel, the multijet background is estimated using a data sample containing events that pass less restrictive electron quality requirements. Both multijet samples are corrected for contributions from processes modeled by MC. The multijet normalizations are determined from fits to the $M_T^{\ell\nu}$ distributions and assigned uncertainties of 20%.

To identify heavy quark (b and c) jets, in particular those originating from Z decays, we use the D0 neural network (NN) b-tagging algorithm [21]. The NN is trained to separate light-flavor jets from heavy-flavor jets based on a combination of variables sensitive to the presence of tracks and vertices displaced from the primary $p\bar{p}$ interaction vertex. The NN outputs for the two highest p_T jets are then used as inputs to the final multivariate discriminant. We define non-overlapping 0, 1, and 2-tag sub-channels based on whether neither, only one, or both of the two highest p_T jets pass the least restrictive NN operating point, for which the b-jet identification efficiency and the light-flavor jet misidentification rate are approximately 80% and 10%. Scale factors are applied to the MC events to account for any difference in efficiency or misidentification rate between data and simulation.

The dominant background is W+jets and therefore the modeling of this process in ALPGEN and the corresponding sources of uncertainties were studied in detail. Comparison of ALPGEN with other generators [22] and with data shows discrepancies in jet η, dijet angular separation and the transverse momentum of the W boson candidate. Thus, data are used to correct these quantities in the ALPGEN W+jets and Z+jets samples before b-tagging is performed [23]. The possible bias in this procedure from the presence of the diboson signal in data is small, but is taken into account as a systematic uncertainty.

As the diboson events are generated with a LO generator, changes to the event kinematics and the acceptance due to a NLO and resummation effects are studied using events from the MC@NLO [24] interfaced to HERWIG [25] for parton showering and hadronization and using the CTEQ6M PDF set. Comparing kinematics at the generator level after final state radiation, we parameterize a two-dimensional correction matrix in the p_T of the diboson system and of the highest p_T boson. After applying this correction to our PYTHIA sample, we find good agreement with MC@NLO for all distributions studied. Half of the difference between the PYTHIA and MCNLO pre-

TABLE I: Number of events for signal and each background after the combined fit of WV using the RF output distribution (with total uncertainties determined from the fit) and the number of events observed in data.

	Electron channel	Muon channel
Diboson signal	1725 ± 84	1465 ± 67
W/Z+light-flavor jets	37232 ± 1033	33516 ± 709
W/Z+heavy-flavor jets	5371 ± 608	4854 ± 490
$t\bar{t}$ and single top	1746 ± 127	1214 ± 86
Multijet	10630 ± 1007	1982 ± 384
Total predicted	56704 ± 635	43031 ± 531
Data	56698	43044

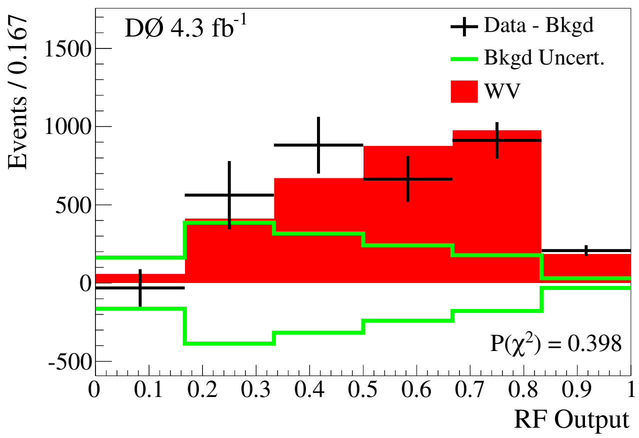

FIG. 1: (color online) A comparison of the measured WV signal (filled histogram) to background-subtracted data (points) in the RF output distribution (summed over electron and muon channels, and 0, 1, and 2-tag sub-channels), after the combined fit to data using the RF output distributions. Also shown is the posterior uncertainty (±1 s.d.) on the subtracted background prediction. The χ^2 fit probability, P(χ^2), is based on the residuals using data and MC statistical uncertainties.

dictions is used as systematic uncertainty on the diboson production model, accounting for the possible effects of higher order corrections beyond NLO and of different showering scenarios.

The signal and the backgrounds are further separated using a multivariate classifier to combine information from several variables. This analysis uses a random forest (RF) classifier [26, 27], from which the output distribution is used as a final variable to measure the production cross sections by performing a template fit. Fifteen well-modeled variables [28] that demonstrate a difference in probability density between signal and at least one of the backgrounds are used as inputs to the RF. Among these variables the invariant mass of the jet pair provides most of the discrimination between signal and background. The RF is trained using a fraction of each MC sample. The remainder of each MC sample, along with the multijet background samples, is then evaluated by the RF and used in the measurement.

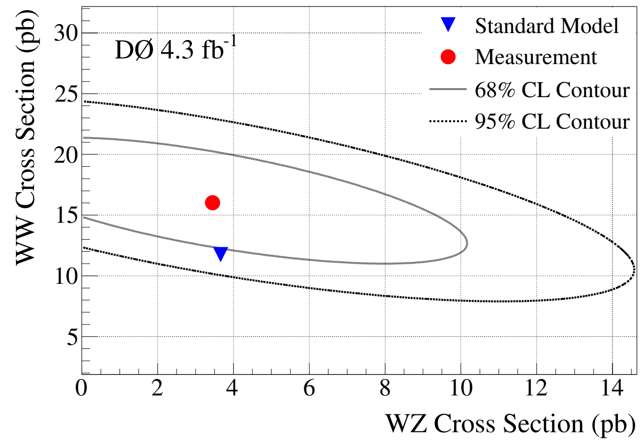

FIG. 2: (color online) Results from the simultaneous fit of $\sigma(WW)$ and $\sigma(WZ)$ using the RF output distributions. The plot shows the best fit value with 68% and 95% confidence level (CL) regions and the NLO SM prediction.

Depending on the source, we consider the effect of systematic uncertainty on the normalization and/or on the shape of differential distributions for signal and backgrounds [28]. Systematic effects on the differential distributions of the ALPGEN W+jets and Z+jets MC events from changes of the renormalization and factorization scales and of the parameters used in the MLM parton-jet matching algorithm [29] are also considered. Uncertainties on PDFs [30], as well as uncertainties from object reconstruction and identification, are evaluated for all MC samples.

The total WV cross section is determined from a fit to the data of the signal and background RF output distributions. The fit is performed simultaneously on the six distributions corresponding to the electron and muon channels and the 0, 1, and 2-tag sub-channels. The fit is performed by minimizing a Poisson χ^2 function with respect to Gaussian priors on each of the systematic uncertainties [31]. The effects on separate samples or subchannels due to the same uncertainty are assumed to be 100% correlated. However, different uncertainties are assumed to be mutually independent. The total posterior uncertainty from the fit, including off-diagonal covariance terms, is reported in Table I. This posterior uncertainty is smaller than the prior uncertainty due to the significant constraint of the data in the region of low RF output, which contains very little expected diboson signal.

The fit simultaneously varies the signal and W+jets contributions, thereby also determining the normalization factor for the W+jets MC sample. This obviates the need for using the predicted ALPGEN cross section, and provides a more rigorous approach that incorporates an unbiased uncertainty from W+jets when extracting the signal cross section. The W+jets normalization factor from the fit is consistent with the theoretical NNLO pre-

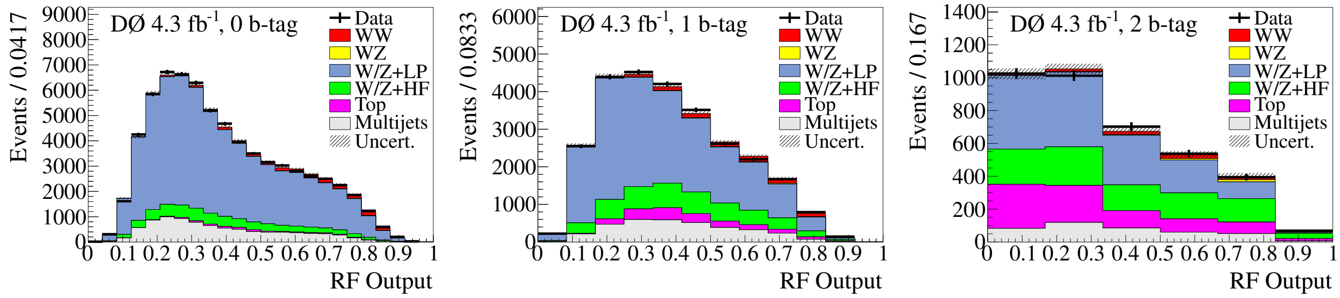

FIG. 3: (color online) A comparison of the signal+background prediction to data in the RF output distribution (summed over electron and muon channels) for 0, 1, and 2-tag sub-channels after the combined fit to data using the RF output distribution (LP denotes light partons such as u, d, s or gluon, and HF denotes heavy-flavor such as $c\bar{c}$ or $b\bar{b}$). The systematic uncertainty band is evaluated after the fit of the total WV cross section in the RF output distribution.

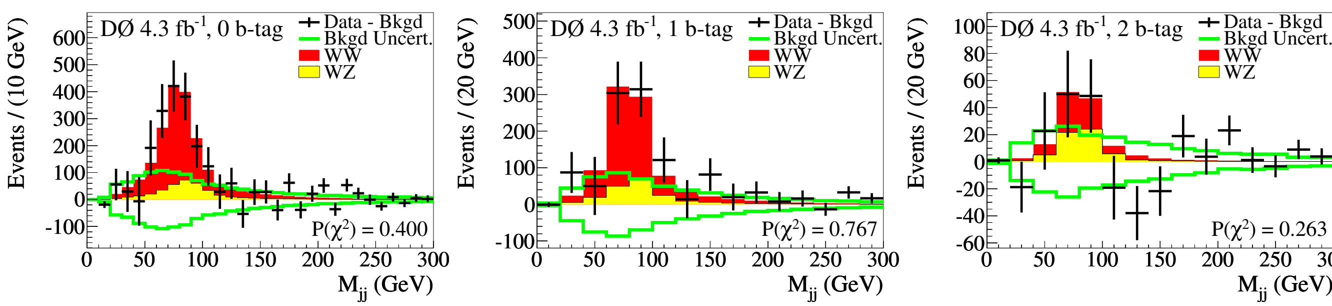

FIG. 4: (color online) A comparison of the measured WW and WZ signals (filled histograms) to background-subtracted data (points) in the dijet mass distribution (summed over electron and muon channels) for 0, 1, and 2-tag sub-channels after the combined fit to data using the dijet mass distribution. Also shown is the posterior uncertainty (± 1 s.d.) on the subtracted background prediction. The χ^2 fit probability, P(χ^2), is based on the residuals using data and MC statistical uncertainties.

diction [32]. The yields for signal and each background are given in Table I. Though the total diboson yield includes a small contribution from $ZZ \rightarrow \ell\ell qq$ events (1.5%), in which one of the charged leptons escapes detection, the cross sections presented here are corrected for this contribution assuming that the ratios between WW, WZ and ZZ cross sections are given by the SM.

The fit of the total WV cross section using the RF output distributions yields $\sigma(WV) = 19.6\ ^{+3.2}_{-3.0}$ pb, corresponding to an observed (expected) significance of 7.9 (5.9) standard deviations (s.d.). Figure 1 shows the background-subtracted RF output distribution summed over all sub-channels after the fit. As a cross check, we perform the measurement using the dijet mass distributions in place of the full RF output distributions [28]. This measurement yields a WV cross section of $\sigma(WV) = 18.3\ ^{+3.8}_{-3.6}$ pb, consistent with that obtained using the RF output distribution.

The fit is then performed with the signal divided into the separate WW and WZ components, which are allowed to float independently. The result of this simultaneous fit of $\sigma(WW)$ and $\sigma(WZ)$ using the RF output distributions is shown in Fig. 2. It yields $\sigma(WW) = 15.9\ ^{+1.9}_{-1.5}$ (stat) $^{+3.2}_{-2.9}$ (syst) pb and $\sigma(WZ) = 3.3\ ^{+3.4}_{-2.7}$ (stat) $^{+2.2}_{-1.8}$ (syst) pb. The RF output distributions for the 0, 1, and 2-tag sub-channels from this fit are shown in Fig. 3. This measurement is also verified fitting the dijet mass distribution, which yields $\sigma(WW) = 13.3\ ^{+2.8}_{-2.2}$ (stat) $^{+3.6}_{-2.9}$ (syst) pb and $\sigma(WZ) = 5.4\ ^{+2.7}_{-2.6}$ (stat) $^{+4.5}_{-4.3}$ (syst) pb. Figure 4 shows plots for the background-subtracted dijet mass after the dijet mass fit.

We also perform a fit in which we constrain the WW cross section to its SM prediction with a Gaussian prior equal to the theoretical uncertainty of 7% [1]. The fit of the RF output distribution yields a WZ cross section of $\sigma(WZ) = 6.5 \pm 0.9$ (stat) $\pm$ 3.0 (syst) pb with observed (expected) significance of 2.2 (1.2) s.d., and the dijet mass fit yields $\sigma(WZ) = 6.7 \pm 1.0$ (stat) $\pm$ 3.9 (syst) pb with observed (expected) significance of 1.7 (0.9) s.d. As expected, now that $\sigma(WW)$ is constrained to the SM prediction, the fit requires a higher rate for WZ in order to account for the excess of signal-like events.

In summary, we have measured the cross section for total WV production to be $\sigma(WV) = 19.6\ ^{+3.2}_{-3.0}$ pb ($V = W$ or Z) with a significance of 7.9 s.d. above the background-only hypothesis. This result demonstrates the ability of the D0 experiment to measure a dijet signal in a background-dominated final state directly relevant to low mass Higgs searches. Furthermore, we have used b-jet tagging to measure the contributions from

WW and WZ and measured the cross sections for the separate processes to be $\sigma(WW) = 15.9\ ^{+3.7}_{-3.2}$ pb and $\sigma(WZ) = 3.3\ ^{+4.1}_{-3.3}$ pb. Although we cannot yet claim 3 s.d. evidence of a WZ signal in the $\ell\nu jj$ final states, the extracted WV and WZ cross sections are in agreement with the SM prediction and their precise measurement represents an independent test to new physics which could manifest itself differently in different final states.

We thank the staffs at Fermilab and collaborating institutions, and acknowledge support from the DOE and NSF (USA); CEA and CNRS/IN2P3 (France); FASI, Rosatom and RFBR (Russia); CNPq, FAPERJ, FAPESP and FUNDUNESP (Brazil); DAE and DST (India); Colciencias (Colombia); CONACyT (Mexico); KRF and KOSEF (Korea); CONICET and UBACyT (Argentina); FOM (The Netherlands); STFC and the Royal Society (United Kingdom); MSMT and GACR (Czech Republic); CRC Program and NSERC (Canada); BMBF and DFG (Germany); SFI (Ireland); The Swedish Research Council (Sweden); and CAS and CNSF (China).

[1] J. M. Campbell and R. K. Ellis, Phys. Rev. D **60**, 113006 (1999). We use MCFM version 6.0.
[2] K. Hagiwara, S. Ishihara, R. Szalapski, and D. Zeppenfeld, Phys. Rev. D **48** (1993).
[3] J. C. Pati and A. Salam, Phys. Rev. D **10**, 275 (1974); **11** 703(E) (1975); G. Altarelli, B. Mele, and M. Ruiz-Altaba, Z. Phys. C **45**, 109 (1989); **47**, 676(E) (1990); H. Davoudiasl, J. L. Hewett, and T. G. Rizzo, Phys. Rev. D **63**, 075004 (2001); H. He *et al.*, Phys. Rev. D **78**, 031701 (2008).
[4] V. M. Abazov *et al.* (D0 Collaboration), Phys. Rev. Lett. **104**, 071801 (2010); V. M. Abazov *et al.* (D0 Collaboration), Phys. Rev. Lett. **105**, 251801 (2010); V. M. Abazov *et al.* (D0 Collaboration), Phys. Lett. B **698**, 6 (2011).
[5] T. Aaltonen *et al.* (CDF Collaboration), Phys. Rev. Lett. **104**, 201801 (2010); V. M. Abazov *et al.* (D0 Collaboration), Phys. Lett. B **695**, 67 (2011); V. M. Abazov *et al.* (D0 Collaboration), Phys. Rev. D **84**, 011103 (2011).
[6] T. Aaltonen *et al.* (CDF Collaboration), Phys. Rev. Lett. **103**, 091803 (2009); T. Aaltonen *et al.* (CDF Collaboration), Phys. Rev. Lett. **104**, 101801 (2010).
[7] S. Chairchyan *et al.* (CMS Collaboration), Phys. Lett. B **699**, 25 (2011); G. Aad *et al.* (ATLAS Collaboration), Phys. Rev. Lett. **107**, 041802 (2011); G. Aad *et al.* (ATLAS Collaboration), arXiv:1111.5570 [hep-ex]; G. Aad *et al.* (ATLAS Collaboration), arXiv:1110.5016 [hep-ex] (2011).
[8] B. Abbott *et al.* (D0 Collaboration), Nucl. Instrum. Methods Phys. Res. A **565**, 463 (2006); M. Abolins *et al.*, Nucl. Instrum. and Methods A **584**, 75 (2007); R. Angstadt *et al.*, Nucl. Instrum. Methods Phys. Res. A **622**, 298 (2010).
[9] D0 uses a spherical coordinate system with the z axis running along the proton beam axis. The angles θ and ϕ are the polar and azimuthal angles, respectively. Pseudorapidity is defined as $\eta = -\ln[\tan(\theta/2)]$, in which θ is measured with respect to the proton beam direction.
[10] G. C. Blazey *et al.*, arXiv:hep-ex/0005012 (2000). The seeded cone algorithm with radius $\Delta\mathcal{R} = \sqrt{(\Delta\eta)^2 + (\Delta\phi)^2} = 0.5$ is used.
[11] J. Smith, W. L. van Neerven, and J. A. M. Vermaseren, Phys. Rev. Lett. **50**, 1738 (1983).
[12] T. Sjöstrand, S. Mrenna and P. Skands, J. High Energy Phys. **05**, 026 (2006). Version 6.409 is used.
[13] J. Pumplin *et al.*, J. High Energy Phys. **07**, 12 (2002); J. Pumplin *et al.*, J. High Energy Phys. **10**, 46 (2003).
[14] M. L. Mangano *et al.*, J. High Energy Phys. **07**, 001 (2003). Version 2.11 is used with the $W+c$ fix from v2.12.
[15] E. Boos *et al.* (CompHEP Collaboration), Nucl. Instrum. Methods Phys. Res. A **534**, 250 (2004).
[16] R. Brun, F. Carminati, CERN Program Library Long Writeup W5013 (1993).
[17] R. Gavin, Y. Li, F. Petriello, and S. Quackenbush, Comput. Phys. Commun. **182**, 2388 (2011).
[18] N. Kidonakis and R. Vogt, Phys. Rev. D **78**, 074005 (2008).
[19] N. Kidonakis, Phys. Rev. D **74**, 114012 (2006).
[20] J. M. Campbell and R. K. Ellis, Phys. Rev. D **65**, 113007 (2002).
[21] V. M. Abazov *et al.* (D0 Collaboration), Nucl. Instrum. Methods Phys. Res. A **620**, 490 (2010).
[22] J. Alwall *et al.*, Eur. Phys. C **53**, 473 (2008).
[23] V. M. Abazov *et al.* (D0 Collaboration), Phys. Rev. Lett. **107**, 011804 (2011).
[24] S. Frixione and B. R. Webber, J. High Energy Phys. **06**, 029 (2002); S. Frixione, P. Nason and B. R. Webber, J. High Energy Phys. **08**, 007 (2003). Version 3.3 is used.
[25] G. Corcella *et al.*, J. High Energy Phys. **01**, 010 (2001).
[26] L. Breiman, Machine Learning **45**, 5 (2001).
[27] I. Narsky, arXiv:physics/0507143 (2005).
[28] See EPAPS Document No. E-PRL for additional material. For more information on EPAPS, see http://www.aip.org/pubservs/epaps.html.
[29] S. Höche *et al.*, arXiv:hep-ph/0602031 (2006).
[30] J. Pumplin *et al.*, Phys. Rev. D **65**, 014013 (2002).
[31] W. Fisher, FERMILAB-TM-2386-E (2006).
[32] R. Hamberg, W. L. van Neerven, and T. Matsuura, Nucl. Phys. B **359**, 343 (1991); **644**, 403 (2002).